Inorg. Chem. **2002**, *41*, 229–238

Dynamic Behavior of the Jahn–Teller Distorted $Cu(H_2O)_6^{2+}$ Ion in Cu^{2+} Doped $Cs_2[Zn(H_2O)_6](ZrF_6)_2$ and the Crystal Structure of the Host Lattice

Michael A. Hitchman,*,† Yurii V. Yablokov,*,‡ Vladimir E. Petrashen,§ Maria A. Augustyniak-Jabłokov,‡ Horst Stratemeier,† Mark J. Riley,|| Kazimierz Łukaszewicz,⊥ Paweł E. Tomaszewski,⊥ and Adam Pietraszko⊥

School of Chemistry, University of Tasmania, Box 252-75 Hobart, TAS 7001 Australia, Institute of Molecular Physics PAS, Smoluchowskiego 17, 60-179 Poznań, Poland, Kazan Physical Technical Institute RAS, Sibirskii trakt 10/7, 420029 Kazan, Russia, Chemistry Department, University of Queensland, St. Lucia, Queensland 4072, Australia, and Institute of Low Temperature and Structure Research, PAS, P. Nr 1410, 50-950 Wrocław, Poland

Received May 1, 2001

The temperature dependence of the X- and Q-band EPR spectra of $Cs_2[Zn(H_2O)_6](ZrF_6)_2$ containing ~1% Cu^{2+} is reported. All three molecular *g*-values vary with temperature, and their behavior is interpreted using a model in which the potential surface of the Jahn–Teller distorted $Cu(H_2O)_6^{2+}$ ion is perturbed by an orthorhombic "strain" induced by interactions with the surrounding lattice. The strain parameters are significantly smaller than those reported previously for the $Cu(H_2O)_6^{2+}$ ion in similar lattices. The temperature dependence of the two higher *g*-values suggests that in the present compound the lattice interactions change slightly with temperature. The crystal structure of the $Cs_2[Zn(H_2O)_6](ZrF_6)_2$ host is reported, and the geometry of the $Zn(H_2O)_6^{2+}$ ion is correlated with lattice strain parameters derived from the EPR spectrum of the guest Cu^{2+} complex.

Introduction

Understanding the mechanisms by which Jahn−Teller (JT) distorted complexes undergo changes in geometry or orientation requires knowledge of the energy and localization of their excited vibronic states.[1−3] For this purpose, a model was developed[4] which calculates the vibronic energy levels of a 6-coordinate copper(II) complex under the influence of 2nd order JT coupling and a lattice strain of orthorhombic symmetry. Initially, this was used to interpret the temperature dependence of the *g*-values of the CuF_6^{4-} complex ion formed when Cu^{2+} is doped into K_2ZnF_4.[4] This system involves a copper(II) complex with the unusual tetragonally compressed octahedral coordination geometry, and the thermal changes in the EPR spectrum are caused by differences in the proportions of the d_{z^2} and $d_{x^2-y^2}$ orbitals in the vibronic wave functions. In this case, the complex undergoes little change in geometry with temperature. The model was subsequently applied[5] to the EPR data for the $Cu(H_2O)_6^{2+}$ ion doped into a range of zinc(II) host lattices, in particular, the Tutton salts of general formula $(cation)_2[Zn(H_2O)_6](SO_4)_2$, where cation represents NH_4, Cs, Rb, and K,[6] and related compounds.[7] In these lattices, the EPR data suggest the copper(II) complex has the more common tetragonally elongated geometry with a significant orthorhombic distortion. The vibronic wave functions confirmed the earlier conclusions of Silver and Getz[3] and Petrashen et al.[6] that to a good approximation the temperature dependence of the *g*-values is caused by a thermal equilibrium between two Jahn−Teller configurations of the $Cu(H_2O)_6^{2+}$ ion with similar *g*-values but for which the directions of the highest and intermediate *g*-values are interchanged. The model was subsequently used to interpret the temperature dependence

* Authors to whom correspondence should be addressed. E-mail: michael.hitchman@utas.edu.au (M.A.H.); yablokov@ifmpan.poznan.pl (Y.V.Y.).
† University of Tasmania.
‡ Institute of Molecular Physics PAS.
§ Kazan Physical Technical Institute RAS.
|| University of Queensland.
⊥ Institute of Low Temperature and Structure Research, PAS.

(1) Sussman, J. A. *J. Phys. Chem. Solids* **1967**, *28*, 1643.
(2) Vikhnin, V. S. *Solid State Phys. (Russian)* **1978**, *20*, 1340.
(3) Silver, B.; Getz, D. *J. Chem. Phys.* **1974**, *61*, 638.
(4) Riley, M. J.; Hitchman, M. A.; Reinen, D. *Chem. Phys*. **1986**, *102*, 11.
(5) Riley, M. J.; Hitchman, M. A.; Mohammed, A. W. *J. Chem. Phys.* **1987**, *87*, 3766.
(6) Petrashen, V. E.; Yablokov, Yu. V.; Davidovich, R. L. *Phys. Status Solidi B* **1980**, *101*, 117.
(7) Ziatdinov, A. M.; Zaripov, M. M.; Yablokov, Yu. V.; Davidovich, R. L. *Phys. Status Solidi B* **1976**, *78*, K69.

10.1021/ic010464d CCC: $22.00
Published on Web 01/03/2002

of the EPR spectra of Cu^{2+} doped into a range of other host lattices[8] and extended to treat the concomitant variations in copper−ligand bond lengths observed for several pure copper(II) compounds,[9] including also the cooperative interactions which sometimes occur for these systems.[10]

We report here our study of the temperature dependence of the EPR spectrum of ~1% Cu^{2+} doped into the compound $Cs_2[Zn(H_2O)_6](ZrF_6)_2$. This follows an earlier report of the dependence of the EPR spectrum on the doping concentration of the Cu^{2+} ion in this host[11] and provides an opportunity to study the properties of the $Cu(H_2O)_6^{2+}$ ion in a crystal lattice which differs somewhat from that of the previously studied Tutton salts. In contrast to the Tutton salts, because the influence of the lattice strain in $Cs_2\{Zn[Cu](H_2O)_6\}(ZrF_6)_2$ is relatively small, the vibronic levels localized in all three minima of the warped Mexican hat potential surface become thermally populated by room temperature. All three *g*-values therefore vary with temperature, allowing the parameters describing the JT potential surface to be defined with considerable accuracy. In addition, the EPR suggests that the lattice interactions with the copper(II) complex vary slightly with temperature, and the line shape changes in an unusual manner. To evaluate properly the influence of the lattice, the crystal structure of $Cs_2[Zn(H_2O)_6](ZrF_6)_2$ was determined, and this is compared with that of the Tutton salts and the analysis of the EPR spectrum.

Experimental Results

Preparation of Compounds. Single crystals of $Cs_2[Zn(H_2O)_6](ZrF_6)_2$ were grown by slow evaporation of an aqueous solution containing a stoichiometric ratio of $ZnZrF_6 \cdot 6H_2O$ and Cs_2ZrF_6 with a small admixture of HF. The $ZnZrF_6 \cdot 6H_2O$ compound was synthesized as described previously,[12] and the Cs_2ZrF_6 compound was synthesized from CsF and $ZrF_4 \cdot 3H_2O$ dissolved in HF in a molar ratio 2:1. The Cu doped crystals were obtained by substitution of the appropriate amount of $ZnZrF_6 \cdot 6H_2O$ for $CuZrF_6 \cdot 4H_2O$ in the water solution. Plastic apparatus was used to prevent corrosion, and the preparation was carried out in a fume hood using rubber gloves.

X-ray Crystal Structure Determination. The crystal structure was determined at 293 K. Preliminary measurements were made on several crystals, all of which were found to exhibit twinning (ferroelastic twins within the sample). The structural data were collected on a nearly single-domain sample using a X-ray single-crystal KM4-CCD four-circle diffractometer (KUMA Diffraction, Wrocław, Poland) with a graphite monochromator and Mo Kα radiation. Experimental details are summarized in Table 1. The lattice parameters were refined using all data recorded from one twin and KUMA KM4-CCD software, version 1.143. The data from the more pronounced twin were extracted with great care. Initially, the recorded reflections were divided, by using the KM4-CCD software, into two sets, corresponding to the two twins present in the sample. During the structure solution made on the data set of one twin only, several reflections affected by the second twin (because of complete or partial overlapping) were omitted from the final calculations. Solution and refinement of the structure was performed with the SHELX-97 program package,[13] and the structure diagram was made using the DIAMOND program.[14] The structure was refined in the monoclinic space group *P*21/*n* (no. 14) with two formula units in the unit cell. This unit cell, which differs from that of the Tutton salts, was chosen to conform with that of the high-temperature orthorhombic cell with the space group *Pmnn* (no. 58) described[15] for the high-temperature modification of the corresponding copper compound $Cs_2[Cu(H_2O)_6](ZrF_6)_2$. All atoms in the structure were found, and the positions as well as their anisotropic displacement factors were refined for non-H atoms; for H atoms, the isotropic displacement factors were refined. Complete listings of atomic coordinates, anisotropic displacement parameters, bond distances and angles, and hydrogen bonds are presented in Tables 2, 3, and 4, respectively. The atomic numbering is shown in Figure 1.

Table 1. Crystal Data and Structure Refinement for $Cs_2[Zn(H_2O)_6](ZrF_6)_2$

empirical formula	$H_{12}Cs_2F_{12}O_6ZnZr_2$
cryst size, mm^3	$0.18 \times 0.24 \times 0.28$
fw	849.73
T, K	293(2)
wavelength, Å	0.710 73
cryst syst	monoclinic
space group	$P2_1/n$ (No. 14)
a, Å	6.9700(10)
b, Å	10.515(2)
c, Å	11.803(2)
β, deg	93.56(3)
V, $Å^3$	863.4(3)
Z	2
calcd density, Mg/m^3	3.269
abs coeff, mm^{-1}	6.852
F(000)	776
θ range for data collection	5.86−27.85°
limiting indices	$-9 \le h \le 9, -13 \le k \le 13, -10 \le l \le 15$
reflns collected/unique	6060/1834 [*R*(int) = 0.0380]
completeness to $\theta = 27.85$	89.2%
refinement method	full-matrix least-squares on F^2
data/parameters	1834/131
GOF on F^2	0.875
final *R* indices [$I > 2\sigma(I)$]	R1 = 0.0405, wR2 = 0.0943
R indices (all data)	R1 = 0.0420, wR2 = 0.0951
extinction coeff	0.0451(12)
largest diff peak and hole, e A^{-3}	1.973 and −0.731

EPR Measurements. EPR measurements were carried out at X-band (~9.3 GHz) and Q-band (~35.4 GHz) frequency in the temperature range 4.2−300 K using ESR-230 and modified RE-1303 spectrometers. Self-constructed equipment was used to make

(8) Riley, M. J.; Hitchman, M. A.; Reinen, D.; Steffen, G. *Inorg. Chem.* **1988**, *27*, 1924. Steffen, G.; Reinen, D.; Stratemeier, H.; Riley, M. J.; Hitchman, M. A.; Matthies, H. E.; Recker, K.; Wallrauffen, F.; Kiklas, J. R. *Inorg. Chem.* **1990**, *29*, 2123. Headlam, H.; Hitchman, M. A.; Stratemeier, H.; Smits, J. M. M.; Beurskens, P. T.; de Boer, E.; Janssen, G.; Gatehouse, B. M.; Deacon, G. B.; Ward, G. N.; Riley, M. J.; Wang, D. *Inorg. Chem.* **1995**, *34*, 5516.

(9) Bebendorf, J.; Bürgi, H.-B.; Gamp, E.; Hitchman, M. A.; Murphy, A.; Reinen, D.; Riley, M. J.; Stratemeier, H. *Inorg. Chem.* **1996**, *35*, 7419. Simmons, C. J.; Hitchman, M. A.; Stratemeier, H.; Schultz, A. J. *J. Am. Chem. Soc.* **1993**, *115*, 11304.

(10) Hitchman, M. A.; Maaskant, W.; van der Plas, J.; Simmons, C. J.; Stratemeier, H. *J. Am. Chem. Soc.* **1999**, *121*, 1488.

(11) Eremin, M. V.; Zavidonov, A. Yu.; Petrashen, V. E.; Yablokov, Yu. V.; Davidovich, R. L. *Solid State Phys. (Russian)* **1987**, *29*, 3426.

(12) Davidovich, R. L.; Levchishina, T. F.; Kaydanova T. A.; Buslaev. Yu. A. *Izv. Acad. Nauk USSR, Neorg. Mater*. **1970**, *6*, 493.

(13) Sheldrick, G. M. *SHELXL97: Program for the solution and refinement of crystal structures*; University of Göttingen: Germany, 1997.

(14) Brandenburg, K.; Berndt, M.; Bergerhoff, G. *DIAMOND: Visual crystal structure information system*, Version 2.1; Crystal Impact: Bonn, Germany, 1999.

(15) Łukaszewicz, K.; Pietraszko, A.; Tomaszewski, P. E.; Augustyniak-Jabłokov, M. A.; Yablokov, Yu. V. *Abstracts of XIV Polish-Czech Seminar: Structural and Ferroelectric Phase Transitions*; Swinoujscie, 2000.

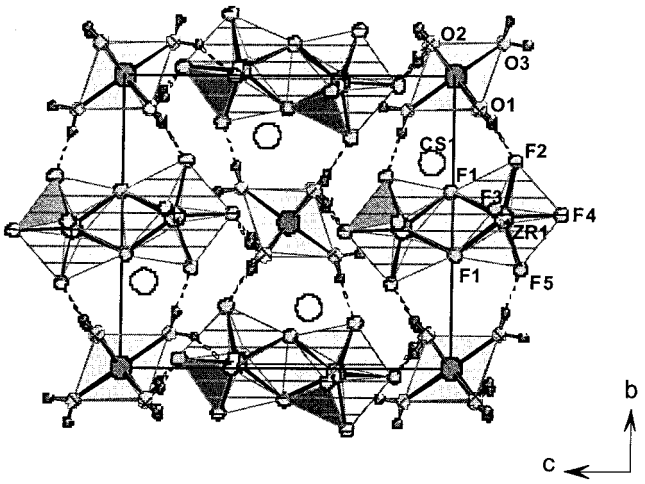

Figure 1. Crystal structure projection along the *a* crystal axis.

measurements in the temperature range 7−300 K at X-band and in the 100−300 K range at Q-band. Spectra at 4.2 and 77 K were measured using Dewars filled with liquid helium and nitrogen, respectively. Some measurements were carried out on a RADIOPAN SE/X-2547 spectrometer using an Oxford Instruments ESR 900 helium flow cryostat. Considerable difficulty was experienced in identifying the direction of the $Cu(H_2O)_6^{2+}$ distortion because of crystal twinning. This was because the smallest and the largest values of the **g**-tensor in one domain correspond to the largest and smallest in the second domain. Determining the **g**-tensor orientation in the crystal lattice therefore required the selection of a single domain crystal. An optical goniometer was used to determine the crystal morphology, and the directions of the principal *g*-axes were deduced from spectra obtained for different orientations of the magnetic field in the (011) plane by a procedure used previously for the Cu^{2+} doped Tutton salts.[16]

Results and Discussion

X-ray Crystal Structure of $Cs_2[Zn(H_2O)_6](ZrF_6)_2$. The crystal structure of $Cs_2[Zn(H_2O)_6](ZrF_6)_2$ at room temperature, illustrated in Figure 1, is isomorphic with that reported at room temperature for $K_2[Cu(H_2O)_6](ZrF_6)_2$,[17] though we have chosen a lattice cell in a different way in order to conform with the orthorhombic phase observed for the corresponding isomorphic pure copper(II) compound, $Cs_2[Cu(H_2O)_6](ZrF_6)_2$, at high temperature.[16,18] The observed domain structure suggests a ferroelastic character for the compound, like that in $Cs_2[Cu(H_2O)_6](ZrF_6)_2$.[16]

The $Zn(H_2O)_6^{2+}$ ion in $Cs_2[Zn(H_2O)_6](ZrF_6)_2$ lies on an inversion center with three slightly different Zn−O distances (Table 3). The basic geometry is similar to that in the analogous Tutton salts. There are, however, significant differences: rather than being isolated anions, the fluorozirconate ions form $Zr_2F_{12}^{4-}$ dimers, and the distortion of the $Zn(H_2O)_6^{2+}$ complex from octahedral symmetry is considerably smaller than that observed in the Tutton salts. For example, the Zn−O distances are 2.110(2), 2.107(2), and 2.061(2) Å in $(NH_4)_2[Zn(H_2O)_6](SO_4)_2$ at 298 K.[19] A marked difference also occurs in the relative orientations of the two complexes in the unit cell. In the Tutton salts, the Zn−O(9) directions of the two $Zn(H_2O)_6^{2+}$ complexes, which correspond to the direction in which the complex is compressed, are approximately parallel. In the present compound, the direction of the metal−ligand bonds of the two complexes all make acute angles: 65.48°, 70.65°, and 71.36° between the Zn−O(1), Zn−O(2), and Zn−O(3) directions, respectively.

Table 2. Atomic Coordinates ($\times 10^4$) and Equivalent Isotropic Displacement Parameters (Å $\times 10^3$), Anisotropic Displacement Parameters[a] (Å^2 $\times 10^3$), and Hydrogen Coordinates ($\times 10^4$) and Isotropic Displacement Parameters (Å^2 $\times 10^3$) for $Cs_2[Zn(H_2O)_6](ZrF_6)_2$

Atomic Coordinates and Equivalent Isotropic Displacement Parameters

	x	*y*	*z*	*U*(eq)[b]
Cs(1)	5007(1)	7050(1)	668(1)	36(1)
Zr(1)	5178(1)	9804(1)	3473(1)	24(1)
Zn(1)	0	10 000	0	28(1)
O(1)	2086(8)	8918(5)	−774(4)	33(1)
O(2)	−2216(7)	8839(5)	−718(4)	32(1)
O(3)	−349(10)	11 165(6)	−1439(5)	48(2)
F(1)	5197(8)	11 099(4)	4916(3)	43(1)
F(2)	4818(7)	7884(4)	3140(3)	36(1)
F(3)	7942(7)	9492(5)	3755(4)	48(1)
F(4)	5130(6)	9695(4)	1723(3)	34(1)
F(5)	5929(9)	11 566(4)	2936(4)	51(1)
F(6)	2357(7)	10 024(5)	3313(4)	50(1)

Anisotropic Displacement Parameters

	U_{11}	U_{22}	U_{33}	U_{23}	U_{13}	U_{12}
Cs(1)	43(1)	32(1)	33(1)	0(1)	−1(1)	−3(1)
Zr(1)	30(1)	22(1)	19(1)	0(1)	0(1)	1(1)
Zn(1)	32(1)	27(1)	24(1)	−1(1)	1(1)	−1(1)
O(1)	33(2)	37(3)	29(2)	−3(2)	6(2)	−4(2)
O(2)	33(2)	30(2)	31(2)	−1(2)	−1(2)	−1(2)
O(3)	75(4)	41(3)	25(2)	6(2)	−7(3)	−16(3)
F(1)	81(3)	26(2)	23(2)	0(2)	8(2)	−6(2)
F(2)	59(3)	24(2)	25(2)	−1(2)	4(2)	−4(2)
F(3)	33(2)	55(3)	56(3)	−9(2)	5(2)	−3(2)
F(4)	47(2)	35(2)	21(2)	−2(2)	4(2)	−1(2)
F(5)	93(4)	27(2)	34(2)	0(2)	11(2)	−8(2)
F(6)	41(2)	67(3)	42(2)	−20(2)	4(2)	2(2)

Hydrogen Coordinates and Isotropic Displacement Parameters

	x	*y*	*z*	*U*(eq)
H(11)	1630(170)	8550(110)	−1080(100)	50(30)
H(31)	30(170)	11 910(120)	−1610(110)	70(40)
H(21)	−1700(200)	8360(140)	−1140(120)	90(40)
H(12)	2850(140)	9500(100)	−1130(80)	40(20)
H(22)	−2960(160)	9270(110)	−1180(100)	60(30)
H(32)	−720(150)	11 060(100)	−2180(100)	50(30)

[a] The anisotropic displacement factor exponent takes the form $-2\pi^2[h^2a \times {}^2U_{11} + ... + 2hka \times b \times U_{12}]$. [b] *U*(eq) is defined as one-third of the trace of the orthogonalized $\mathbf{U}_{ij}$ tensor.

EPR Spectra. It is convenient to illustrate the way in which the EPR spectrum of $Cs_2\{Zn[Cu](H_2O)_6\}(ZrF_6)_2$ varies with temperature at X- and Q-band frequency using the spectra of a powdered sample shown in Figures 2 and 3. The *g*-values at room temperature were obtained from single-crystal spectra. The direction corresponding to the largest *g*-value, $g_{max} = 2.506$ at 4.2 K, is parallel to the Zn−O(2) bond (the longest in the $Zn(H_2O)_6^{2+}$ complex (see Table 3)) and is larger than that observed in Tutton salts and hydrates

(16) Augustyniak, M. A.; Usachev, A. E. *J. Phys.: Condens. Matter* **1999**, *22*, 4391.
(17) Fischer, J.; Weiss, R. *Acta Crystallogr.* **1973**, *B29*, 1137.
(18) Łukaszewicz, K.; Pietraszko, A.; Tomaszewski, P. E.; Augustyniak-Jabłokov, M. A.; Yablokov, Yu. V. To be published.
(19) Simmons, C. J.; Hitchman, M. A.; Stratemeier, H. *Inorg. Chem.* **2000**, *39*, 6124.

Table 3. Bond Lengths (Å) and Angles (deg) for $Cs_2[Zn(H_2O)_6](ZrF_6)_2$[a]

Zr(1)−F(3)	1.963(5)
Zr(1)−F(6)	1.977(5)
Zr(1)−F(5)	2.038(5)
Zr(1)−F(4)	2.067(4)
Zr(1)−F(2)	2.069(4)
Zr(1)−F(1)#1	2.156(4)
Zr(1)−F(1)	2.181(4)
Zr(1)−Zr(1)#1	3.6530(13)
Zn(1)−O(3)	2.096(5)
Zn(1)−O(3)#2	2.096(5)
Zn(1)−O(1)	2.099(5)
Zn(1)−O(1)#2	2.099(5)
Zn(1)−O(2)#2	2.105(5)
Zn(1)−O(2)	2.105(5)
O(3)−Zn(1)−O(1)	90.7(2)
O(3)#2−Zn(1)−O(1)	89.3(2)
O(3)−Zn(1)−O(1)#2	89.3(2)
O(3)#2−Zn(1)−O(1)#2	90.7(2)
O(3)−Zn(1)−O(2)#2	91.9(2)
O(3)#2−Zn(1)−O(2)#2	88.1(2)
O(1)−Zn(1)−O(2)#2	88.8(2)
O(1)#2−Zn(1)−O(2)#2	91.2(2)
O(3)−Zn(1)−O(2)	88.1(2)
O(3)#2−Zn(1)−O(2)	91.9(2)
O(1)−Zn(1)−O(2)	91.2(2)
O(1)#2−Zn(1)−O(2)	88.8(2)

[a] Symmetry transformations used to generate equivalent atoms: #1, $-x+1, -y+2, -z+1$; #2, $-x, -y+2, -z$.

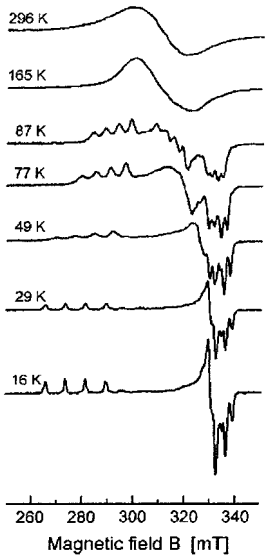

Figure 2. Temperature dependence of the EPR spectrum of powdered $Cs_2\{Zn[Cu](H_2O)_6\}(ZrF_6)_2$ at X-band frequency.

of trigonal symmetry.[3,5−7] That direction associated with the intermediate value, $g_{int} = 2.100$, is parallel to the shortest Zn−O(3) bond, while that parallel to the lowest, $g_{low} = 2.077$, corresponds to Zn−O(1). At low temperature, the spectra are thus characteristic of a **g**-tensor of near axial symmetry. Hyperfine structure due to coupling with the copper nuclear spin $I = {}^3/_2$ splits the resonances of the highest and lowest *g*-values. As the temperature is raised, the low-field resonance corresponding to g_{max} and the resonance due to the g_{int}-value broaden and start to converge at quite low temperature. At X-band, this broadening is most pronounced at ∼50 K, with the peaks becoming better resolved again in the region 80−100 K, before becoming so broad that the hyperfine structure is lost above ∼130 K (Figure 2). At

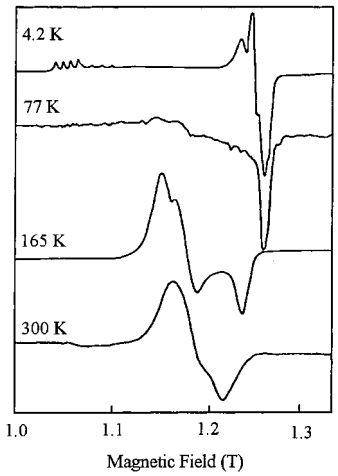

Figure 3. Temperature dependence of the EPR spectrum of powdered $Cs_2\{Zn[Cu](H_2O)_6\}(ZrF_6)_2$ at Q-band frequency.

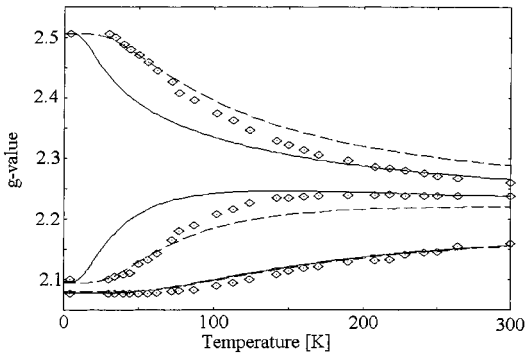

Figure 4. Temperature dependence of the *g*-values of $Cs_2\{Zn[Cu](H_2O)_6\}(ZrF_6)_2$. The lines are values calculated by the model of vibronic coupling as described in the text with values of the orthorhombic component of the lattice strain of 20 cm^{-1} (full lines) and 50 cm^{-1} (dashed lines).

Q-band, the sharp resonances at 4.2 K become so broad they almost disappear at 77 K in the powder spectrum and become hardly detectable for the single crystal, before reappearing as broad peaks again at higher temperatures (Figure 3). The resonance due to the lowest *g*-value also moves to lower field as the temperature is increased, though this commences at relatively high temperature, ∼80 K. The net result of these shifts and the signal broadening is that by room temperature a single broad, asymmetric signal characteristic of a **g**-tensor with a rather small anisotropy and $g_{max} = 2.26 \pm 0.02$, $g_{int} = 2.24 \pm 0.02$, and $g_{low} = 2.16 \pm 0.01$ is observed. The behavior of the *g*-values, as measured at X-band frequency in the range 4.2−130 K, and Q-band above 77 K, is shown in Figure 4.

The thermal behavior of the EPR spectrum of $Cs_2\{Zn[Cu](H_2O)_6\}(ZrF_6)_2$ has some features in common both with those reported for the Cu^{2+} doped Tutton salts[3,5,6] and with those of Cu^{2+} doped $[Zn(H_2O)_6]XF_6$, X = Si[20] and Zr.[7,21] The Cu^{2+} doped Tutton salts show a smooth convergence of just the two higher *g*-values in the temperature range 50−300 K, with the signals progressively broadening as the

(20) Dang, F. S.; Buisson, R.; Williams, F. I. B. *J. Phys. (Paris)* **1974**, *35*, 49.
(21) Ziatdinov, A. M.; Zaripov, M. M.; Yablokov, Yu. V. VINITI, Deponent **30.08.77** *N355*; Ref. *J. Phys.* **1978**, *N1*, 1d734.

temperature rises. The lowest *g*-value of the $Cu(H_2O)_6^{2+}$ ion in the Tutton salt host does not change below ~300 K because the lattice strain interaction has a large negative component (corresponding to a compression of the octahedral site) acting along one of the metal−ligand bond directions, so that the vibronic wave function corresponding to the axial elongation of the bonds along this direction is too high in energy to be thermally populated at room temperature.[3,5,6] The convergence of the two higher *g*-values is due to thermal population of the vibronic wave function localized largely in the second minimum of the warped Mexican hat potential surface, with the rate of exchange between the wave functions always being so rapid that the signal corresponds to the weighted average of the two wave functions.[3] The $[Zn(H_2O)_6]XF_6$ host (X = Si and Zr), on the other hand, has trigonal symmetry, so that, except for the effects of small random strains, the wave functions localized in the three minima of the Mexican hat potential surface of the $Cu(H_2O)_6^{2+}$ ion are equal in energy. At 4.2 K, the rate of exchange between the three lowest energy levels is relatively slow, and the EPR spectrum is the superposition of the three spectra of the three lowest vibronic wave functions. Each has a **g**-tensor corresponding to a tetragonally elongated octahedral coordination geometry but with the long bonds along a different axis.[20−22] When the temperature is raised, the signals broaden and almost disappear in the region 30−60 K, where the rate of exchange is comparable to the EPR time scale. Above ~60 K, the **g**-tensor is quite isotropic because the rate of exchange between the three vibronic wave functions becomes more rapid than the frequency difference between their EPR signals so that an exchange-averaged spectrum is observed.

The most important factor deciding the thermal behavior of the EPR spectrum of the $Cu(H_2O)_6^{2+}$ ion in these lattices is the influence of the host lattice, in particular, the magnitude of the strain interactions which perturb the warped Mexican hat potential surface and discriminate energetically between the directions along which the JT distortion can occur. For $Cs_2\{Zn[Cu](H_2O)_6\}(ZrF_6)_2$, these interactions are considerably weaker than in the Tutton salts, though still much larger than the residual random strains present in the trigonal $Zn(H_2O)_6XF_6$ lattices. This means that for $Cs_2\{Zn[Cu](H_2O)_6\}(ZrF_6)_2$ all three potential energy minima become thermally populated by room temperature, rather than just two as for the doped Tutton salts. All three *g*-values therefore change as a function of temperature. The smooth change in the *g*-values suggests that these correspond to the averaged values of the populated wave functions, as is the case for the doped Tutton salts. On the other hand, the change in line shape of the EPR spectrum of $Cs_2\{Zn[Cu](H_2O)_6\}(ZrF_6)_2$ with temperature is somewhat similar to that observed for the Cu^{2+} doped $Zn(H_2O)_6XF_6$ hosts,[20−22] suggesting similarities in the thermal behavior of the exchange rate between the vibronic wave functions.

In general terms, the extreme broadening of the Q-band EPR spectrum of $Cs_2\{Zn[Cu](H_2O)_6\}(ZrF_6)_2$ at ~77 K in Q-band suggests that at this microwave frequency and temperature the frequency difference of the resonances is comparable to the rate of exchange between the wave functions giving rise to the signals.[23] However, a detailed explanation of the influence of temperature and microwave frequency upon the line shape requires further study, and we are carrying out further work on this aspect.

The values of the lattice strains are reflected in the distortions exhibited by the $Zn(H_2O)_6^{2+}$ ions in the host lattices. These are conveniently measured by the parameter ρ used to describe the JT radius of distortion of a six-coordinate copper(II) complex:[24]

$$\rho = \sqrt{(2\delta x^2 + 2\delta y^2 + 2\delta z^2)} \qquad (1)$$

For a typical zinc(II) Tutton salt, $(NH_4)_2[Zn(H_2O)_6](SO_4)_2$, $\rho = 0.055$ Å,[19] while for $Cs_2[Zn(H_2O)_6](ZrF_6)_2$, it is only 0.009 Å (Table 3). A basic feature of the $Cs_2[Zn(H_2O)_6](ZrF_6)_2$ lattice is, therefore, the rather small anisotropy of the lattice forces acting on the hydrate complex. The EPR spectrum may be used to estimate the lattice interactions perturbing the copper(II) complex, as discussed below, though these may differ somewhat from those acting on the $Zn(H_2O)_6^{2+}$ ion because of the different shapes of the copper and zinc complexes.

Potential Surface and Vibronic Energy Levels of the Copper(II) Complex. The nature of the "warped Mexican hat" potential surface resulting from Jahn−Teller vibronic coupling for a 6-coordinate copper(II) complex, and the way in which this is perturbed by interactions with the surrounding lattice, has been discussed extensively.[24−26] The basic parameters defining the potential surface of the $Cu(H_2O)_6^{2+}$ ion in the absence of lattice perturbations, and the way in which these were estimated, have been described previously.[5] These parameters

$$A_1 = 900\ \text{cm}^{-1};\quad h\nu_{JT} = 300\ \text{cm}^{-1};\quad \beta = \sim 300\ \text{cm}^{-1}$$

have been used to interpret successfully the temperature dependence of the **g**-tensors observed for this complex ion in a range of zinc(II) Tutton salts and similar lattices[5−7] and were therefore taken as the starting point in the present calculations. Here, the linear JT coupling coefficient A_1 and the energy of the Jahn−Teller active vibration $h\nu_{JT}$ are both known quite accurately from spectroscopic studies.[5] However, the parameter β, which describes the energy by which the minima of the basic warped Mexican hat potential surface are stabilized by higher-order effects, was much less well defined, the uncertainty being $\sim\pm 150$ cm^{-1}.[5] A major purpose of the present study was, therefore, to estimate this parameter more reliably.

(22) Abragam, A.; Bleaney, B. *Electron Paramagnetic Resonance of Transition Metal Ions*; Clarendon: Oxford, 1970; p 460.

(23) Carrington, A.; McLachlan, A. D. *Introduction to Magnetic Resonance*; Harper & Row: New York, 1967; Chapter 12.

(24) Reinen, D.; Friebel, C. *Struct. Bonding (Berlin)* **1979**, *37*, 1. Reinen, D.; Atanasov, M. *Magn. Reson. Rev.* **1991**, *15*, 167.

(25) Yablokov, Yu. V.; Usachev, A. E.; Ivanova, T. A.; *Radiospectroscopy of Condenced Matter*; Zaripov, M. M., Ed. Moscow: Science, 1990. Petrashen, V. E. Ph.D. Thesis, Kazan University, 1985.

(26) Hitchman, M. A. *Comments Inorg. Chem.* **1994**, *15*, 197. Reinen, D.; Hitchman, M. A. *Z. Phys. Chem.* **1997**, *200*, 11.

The temperature dependence of the *g*-values is due to the perturbation of the potential surface by lattice interactions, which are represented by the axial and orthorhombic strain components S_θ and S_ϵ. These render the three minima of the warped Mexican hat potential surface inequivalent. Provided that, as in the present systems, the strain is small compared with β, it has little effect on the position of the minima in the potential surface. The energy of the highest well relative to the lowest is decided largely by S_θ, while that of the intermediate well is influenced mainly by S_ϵ. Provided the warping of the potential surface is relatively large, as is the case for the $Cu(H_2O)_6^{2+}$ ion, it follows that the temperature dependence of the highest and intermediate *g*-values depends mainly upon S_ϵ, while that of the lowest *g*-value is decided largely by S_θ.[5,26] When $S_\theta < 0$, the ratio of β to S_θ strongly influences the position of the lowest energy minimum in the warped Mexican hat potential surface, and, hence, the anisotropy of the *g*-values of the lowest vibronic wave function.[5,26,27] This means that if the axial strain is well defined, the warping parameter may be deduced accurately also.

The above constraints were used to fit the *g*-values of $Cs_2\{Zn[Cu](H_2O)_6\}(ZrF_6)_2$, and in the low-temperature region (4−70 K), good agreement with experiment was obtained using the warping and strain parameters:

$$\beta = 225\ \text{cm}^{-1};\quad S_\theta = -100\ \text{cm}^{-1};\quad S_\epsilon = 50\ \text{cm}^{-1}$$

as shown by the dashed lines in Figure 4. Here, the negative sign for S_θ means that the strain acts as a compression. Excited-state energies $E(^2T_2g) = 11\,000\ \text{cm}^{-1}$, linear coupling constant $A_1(^2T_{2g})$ of the excited state $-450\ \text{cm}^{-1}$, and orbital reduction parameters $k_x = 0.875$, $k_y = 0.87$, and $k_z = 0.85$ were used to estimate the *g*-values from the electronic components of the vibronic wave functions. These values are quite similar to those giving optimum agreement with the experimental data of the Cu^{2+} doped Tutton salts ($E(^2T_{2g}) = 11\,900\ \text{cm}^{-1}$, $A_1(^2T_{2g}) = -330\ \text{cm}^{-1}$, $k_x = k_y = k_z = 0.88$.[5] Because for $Cs_2\{Zn[Cu](H_2O)_6\}(ZrF_6)_2$, the lowest *g*-value starts to rise as the temperature increases above ~70 K, the axial strain, S_θ, and β may be determined relatively accurately, with a change in either parameter of ~15% causing a noticeable worsening of the fit. This is in contrast to the doped Tutton salts, where the lowest *g*-value shows no temperature dependence in the available temperature region,[6] so that the axial strain, and, hence, the warping parameter β, could only be estimated rather approximately.[5]

Although the above parameters provide a satisfactory fit for the temperature dependence of the *g*-values of $Cs_2\{Zn[Cu](H_2O)_6\}(ZrF_6)_2$ in the low temperature region, the two higher *g*-values converge more rapidly than the model predicts at higher temperature (70−300 K, Figure 4). The *g*-values above ~160 K may be reproduced satisfactorily assuming an identical set of parameters except for a slightly smaller value of the orthorhombic strain, $S_\epsilon = 20\ \text{cm}^{-1}$, as indicated by the solid lines in Figure 4. The behavior of the *g*-values over the whole temperature range may, therefore, be reproduced satisfactorily assuming that perturbations of a potential surface due to the host lattice are much smaller than those for the $Cu(H_2O)_6^{2+}$ doped into the Tutton salts[5] and the orthorhombic component of this lattice interaction decreases slightly as the temperature increases.

Another possible explanation for the unusual behavior of the two higher *g*-values could be that cooperative interactions between the copper(II) complexes occur. The cooperative interactions in the $Cs_2\{Zn[Cu](H_2O)_6\}(ZrF_6)_2$ system are due to coupling via the phonon field,[11] so the possibility of long distance cooperative interactions should not be ignored. The EPR study of the concentration dependence of the spectra in $Cs_2\{Zn[Cu](H_2O)_6\}(ZrF_6)_2$ shows that cooperative interactions do take place, but only where the copper content is in the range 40−60%, not at lower doping levels of copper.[11] There is also no evidence of an unequal distribution of Cu^{2+} in the crystal leading to the pair formation. Moreover, as shown elsewhere,[28] although an additional stabilization of the lowest JT configuration of $\sim 25\ \text{cm}^{-1}$ takes place in $K_2\{Zn_{0.92}[Cu_{0.08}](H_2O)_6\}(SO_4)$, this does not influence the behavior of the isolated Cu complexes**.** The most plausible explanation for the anomalous behavior of $Cs_2\{Zn[Cu](H_2O)_6\}(ZrF_6)_2$ is that the lattice changes slightly as the temperature is raised, probably as a result of changes in the hydrogen bonding interactions. It has also been observed that for $(NH_4)_2[M(H_2O)_6](SO_4)_2$, M = Zn and Mg, the orthorhombic distortion of the metal−ligand bond lengths decreases slightly on warming from ~100 to 300 K.[19,29]

A convenient way of representing the potential surface of the $Cu(H_2O)_6^{2+}$ ion is by plotting the energy as a function of Jahn−Teller angle ϕ which is defined by the following linear combination of the two components Q_θ, Q_ϵ of the Jahn−Teller active vibration:[24,26] Here, ρ is the radial

$$Q_\theta = \rho\cos\phi;\quad Q_\epsilon = \rho\sin\phi$$

displacement in the Jahn−Teller mode. The energy of this circular trough of the "Mexican hat" potential surface, calculated by the method in ref 5 at the JT radius ρ of the energy minimum, is shown for the $Cu(H_2O)_6^{2+}$ ion in $Cs_2\{Zn[Cu](H_2O)_6\}(ZrF_6)_2$ in Figure 5. The full line corresponds to the orthorhombic strain at low temperature, $S_\epsilon = 50\ \text{cm}^{-1}$, while the dashed line corresponds to that at higher temperatures, $S_\epsilon = 20\ \text{cm}^{-1}$. The very close similarity between the lines shows that the surface changes very little with temperature. The effect is only detected because the orthorhombic component of the strain is so small in this system.

The model may be used to estimate the ligand displacements which lattice strain terms S_θ, S_ϵ similar to those acting on the $Cu(H_2O)_6^{2+}$ ion would cause in a non-Jahn−Teller active complex such as $Zn(H_2O)_6^{2+}$.[5] For the strain parameters suggested by the *g*-values at lower temperature, $S_\theta = -100$ and $S_\epsilon = 50\ \text{cm}^{-1}$, these ligand displacements are

$$\delta x = 0.0045\ \text{Å};\quad \delta y = 0.0003\ \text{Å};\quad \delta z = -0.0048\ \text{Å} \quad (2)$$

(27) Reinen, D.; Krause, S. *Inorg. Chem.* **1981**, *20*, 2750.

(28) Augustyniak-Jabłokov, M. A.; Yablokov, Yu. *Solid State Commun.* **2000**, *115*, 439.

(29) Simmons, C.; Hitchman, M. A.; Stratemeier, H. Unpublished results.

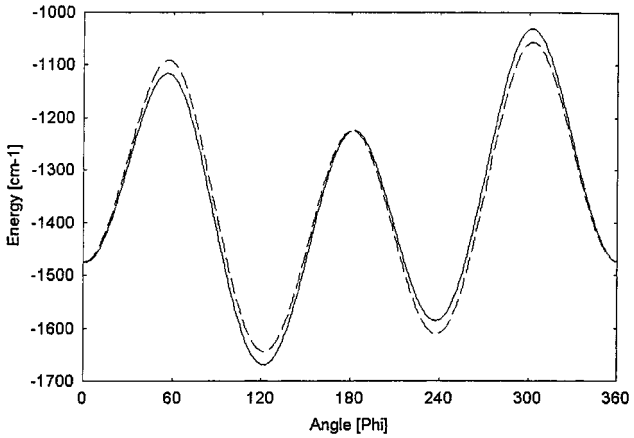

Figure 5. Circular sections through the potential surface at the radial Jahn−Teller distortion corresponding to the energy minimum for the $Cu(H_2O)_6^{2+}$ ion in $Cs_2\{Zn[Cu](H_2O)_6\}(ZrF_6)_2$ for orthorhombic components of the lattice strain $S_\epsilon = 50$ cm^{-1} (full line) and $S_\epsilon = 20$ cm^{-1} (dashed line); see text for the parameters used in the calculation.

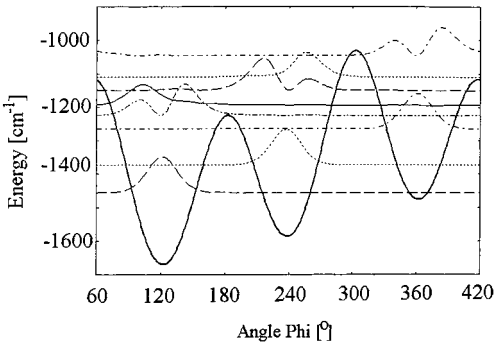

Figure 6. Circular section through the potential surface at the radial Jahn−Teller distortion corresponding to the energy minimum for the $Cu(H_2O)_6^{2+}$ ion in $Cs_2\{Zn[Cu](H_2O)_6\}(ZrF_6)_2$ for an orthorhombic component of the lattice strain $S_\epsilon = 50$ cm^{-1}; see text for the parameters used in the calculation. The squares of the vibrational components of the first eight vibronic wave functions are shown. The contribution from the vibrational motion in the radial direction to the zero-point energy has not been subtracted from the energy levels, as is sometimes done in such plots.[5]

while for those deduced from the EPR at higher temperatures, $S_\theta = -100$ cm^{-1} and $S_\epsilon = 20$ cm^{-1}, they are

$$\delta x = 0.0032 \text{ Å}; \quad \delta y = 0.0016 \text{ Å}; \quad \delta z = -0.0048 \text{ Å} \qquad (3)$$

The changes in bond lengths with temperature implied by the EPR analysis are very small, being less than the standard deviations of the bond lengths (Table 3).

The deviations observed for the hexahydrate ion in $Cs_2[Zn(H_2O)_6](ZrF_6)_2$ at 293 K are

$$\delta_{(Zn-O1)} = -0.001 \text{ Å}; \quad \delta_{(Zn-O2)} = 0.005 \text{ Å}; \quad \delta_{(Zn-O3)} = -0.004 \text{ Å} \qquad (4)$$

The overall distortion ρ (eq 1) to be expected from the strain parameters derived from the EPR analysis is 0.0093 Å at low temperature and 0.0085 Å at high temperature. The distortion, thus, does not change much with temperature and is very close to the value of 0.009 Å observed for the zinc host at 293 K. The orientation of the **g**-tensor with respect to the $Zn(H_2O)_6^{2+}$ ion means that the largest, intermediate, and smallest *g*-values are approximately parallel to the Zn−O2, Zn−O3, and Zn−O1 bonds, respectively. For an orthorhombically distorted copper(II) complex, the magnitudes of the *g*-values correlate with the metal−ligand bond lengths;[30] that is, the highest *g*-value is associated with the longest Cu−L bond, and so forth, so that the Zn−O bond lengths should follow the sequence Zn−O2 > Zn−O3 > Zn−O1 if similar lattice strain parameters act on the host zinc complex as on the guest copper complex. The long axis of the Jahn−Teller distorted guest $Cu(H_2O)_6^{2+}$ ion does indeed correspond to Zn−O2, the direction of the weakest lattice perturbation acting on the host zinc complex. However, the Zn−O1 bond is slightly longer than that to O3, so the directions of the short and intermediate Cu−O bonds do not match those of the zinc complex (though it should be noted that the differences in bond lengths for the zinc complex are less than their uncertainty). Because the Cu-$(H_2O)_6^{2+}$ and $Zn(H_2O)_6^{2+}$ ions have different shapes, this is not a contradiction, because the complexes will interact with the surrounding lattice in a different manner. A structural study of the isomorphous $Cs_2[Cu(H_2O)_6](ZrF_6)_2$ compound[15,18] shows an elongation of the octahedron in the Cu−O2 direction at 150 K, which switches to the Cu−O3 direction above 260K, with the shortest distance at both temperatures corresponding to a compression along the Cu−O1 direction. This implies that the lattice strain interactions are sensitive not only to the nature of the metal ion, but also to temperature. In the Cu^{2+} doped zinc(II) Tutton salts, the direction of the relatively large dominant axial compression ($S_\theta = \sim -500$ cm^{-1}) derived from the EPR[5] has always been found to coincide with the shortest Zn−O bond of the host zinc complex,[5,8,9] but this is not always the case for the small orthorhombic distortion. For Cu^{2+} doped $K_2[Zn(H_2O)_6](SO_4)_2$, this distortion is in the opposite direction to that implied by the strain deduced from the EPR spectrum of Cu^{2+} doped into this host lattice.[3,31] For $Cs_2\{Zn[Cu](H_2O)_6\}(ZrF_6)_2$, both the tetragonal and orthorhombic lattice distortions are very small and apparently do not play a decisive role in determining the structure of the doped $Cu(H_2O)_6^{2+}$ ion.

A useful picture of the structures involved in the dynamic behavior is provided by plots of the squares of the nuclear components of the vibronic wave functions. These are shown in Figure 6 for the first eight levels for a circular section through the potential surface of the $Cu(H_2O)_6^{2+}$ ion in $Cs_2\{Zn[Cu](H_2O)_6\}(ZrF_6)_2$ at low temperature. The three lowest levels are each strongly localized in a different minimum of the warped potential surface. To a good approximation, the fourth, sixth, and eighth wave functions correspond to the first excited vibrational levels of the first three wave functions. Again, these are strongly localized in the three minima, though the inequivalence of the two maxima of each wave function indicates that some delocalization occurs. These wave functions represent vibrations of excited levels

(30) Hitchman, M. A. *J. Chem. Soc. A* **1970**, 4.

(31) Whitnall, J.; Kennard, C. H. L.; Nimmo, J.; Moore, F. H. *Cryst. Struct. Commun.* **1975**, *4*, 717. Ref 5 is in error on this aspect.

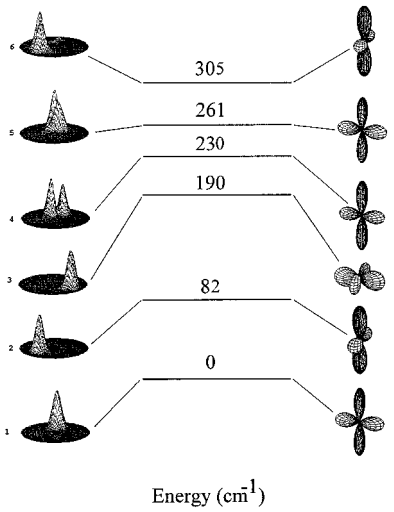

Figure 7. Plots of the squares of the first six vibronic wave functions for the $Cu(H_2O)_6^{2+}$ ion in $Cs_2\{Zn[Cu](H_2O)_6\}(ZrF_6)_2$ for an orthorhombic component of the lattice strain $S_\epsilon = 50$ cm^{-1}. The vibrational components are shown on the left, and the electronic components, on the right.

of the "angular" component of the Jahn−Teller mode.[4] This corresponds to a vibrational motion that produces an orthorhombic geometry.[24,26] The fifth and seventh levels represent the first excited vibrational states of the two lower wave functions; this time, they are in the radial component of the Jahn−Teller active vibration of the parent complex. For this vibration, just a single peak is observed in this circular plot because the wave functions extend radially away from the center of the Mexican hat potential surface.

A more complete picture of the vibrational wave functions is provided by the probability plots in two vibrational dimensions: Q_θ, Q_ϵ, or equivalently ρ, ϕ. These are shown, together with their relative energies, for the first six levels on the left side of Figure 7. Here, it may be seen that the fifth wave function consists of two peaks with the disposition expected for the radial component of the first excited vibrational level of the lowest state. The corresponding probability plots for the electronic components of the vibronic wave functions are shown on the right side of Figure 7. To a good approximation, the first three levels correspond to $d_{x^2-y^2}$-type orbitals with different orientations and very little admixture of a d_{z^2}-type component. This is consistent with the small orthorhombic component of the **g**-tensor at low temperature.[30] For the lowest level, the lobes of the wave function are at right angles to the direction of the smallest component of the lattice strain. This means that the filled d_{z^2}-type orbital associated with the longest Cu−O bonds is directed toward the portion of the lattice which can best accommodate the elongation of the Jahn−Teller distortion. For the second and third wave functions, the change in orientation of the orbital lobes points the long axis of the Jahn−Teller distorted $Cu(H_2O)_6^{2+}$ ion toward the directions of the middle and largest lattice strain components, respectively. The electronic components of the fourth and fifth wave functions look very similar to those of the lowest level, as expected for the two components of the first excited vibrational state of this two-dimensional minimum.

Table 4. Hydrogen Bonds for $Cs_2[Zn(H_2O)_6](ZrF_6)_2$ (Å and deg)[a]

D−H···A	d(D−H)	d(H···A)	d(D···A)	∠(DHA)
O(1)−H(11)···F(2)#2	0.60(12)	2.14(13)	2.735(7)	169(15)
O(3)−H(31)···F(5)#4	0.85(13)	1.82(13)	2.666(8)	175(12)
O(2)−H(21)···F(2)#2	0.82(15)	1.90(15)	2.711(7)	169(14)
O(1)−H(12)···F(4)#5	0.93(10)	1.81(10)	2.723(7)	164(9)
O(1)−H(12)···F(5)#5	0.93(10)	2.60(10)	3.020(7)	108(7)
O(2)−H(22)···F(4)#3	0.86(12)	1.94(12)	2.758(7)	159(11)
O(2)−H(22)···F(6)#3	0.86(12)	2.69(11)	3.284(7)	128(9)
O(3)−H(32)···F(6)#3	0.90(11)	2.05(11)	2.833(7)	145(9)
O(3)−H(31)···F(1)#4	0.85(13)	2.76(13)	3.302(8)	123(10)
O(2)−H(21)···F(1)#1	0.82(15)	2.93(14)	3.318(7)	111(11)
O(3)−H(32)···F(3)#5	0.90(11)	2.83(11)	3.366(8)	120(8)

[a] Symmetry transformations used to generate equivalent atoms: #1, $-x + {}^1/_2, y - {}^1/_2, -z + {}^1/_2$; #2, $x - {}^1/_2, -y + {}^3/_2, z - {}^1/_2$; #3, $-x, -y + 2, -z$; #4, $x - {}^1/_2, -y + {}^5/_2, z - {}^1/_2$; #5, $-x + 1, -y + 2, -z$.

Table 5. g-Values and Relative Energies E of the First Six Levels of the Potential Surfaces with Values of the Orthorhombic Component of the Lattice Strain

level	E,[a] cm^{-1}	g-values[a]			E,[b] cm^{-1}	g-values[b]		
1	0	2.506	2.094	2.08	0	2.506	2.096	2.078
2	82	2.101	2.502	2.075	33	2.100	2.502	2.076
3	190	2.095	2.083	2.487	165	2.091	2.086	2.487
4	230	2.48	2.119	2.072	226	2.453	2.146	2.066
5	261	2.491	2.094	2.09	256	2.296	2.26	2.083
6	305	2.147	2.453	2.064	266	2.314	2.241	2.085

[a] $S_\theta = 50$ cm^{-1}. [b] $S_\theta = 20$ cm^{-1}.

The influence of lattice strain on the position and relative energies of the minima in the JT surface has been discussed in detail elsewhere.[5,26,32] When such strain interactions are very small, the higher-order terms which warp the potential surface, parametrized by β, favor minima at $\phi = 0°$, 120°, and 240°, each of which corresponds to a tetragonally elongated octahedral geometry. An axial compression shifts the minima from these positions, and it has been shown that the ratio $|S_\theta/\beta|$ must exceed 9 for the lowest energy minimum to correspond to a compressed tetragonal geometry.[27,32] When $|S_\theta/\beta| < 9$, an orthorhombic geometry and **g**-tensor occur. In the present case, $S_\theta = -100$ cm^{-1} and $\beta = 225$ cm^{-1}, so the ratio, 0.44, is quite small, and the orthorhombic distortion associated with the lowest vibronic wave functions is minimal. The orthorhombic strain S_ϵ is also very small, so this has little influence on the geometry.

The principal g-values of the first six levels are shown in Table 5 for the potential surface in the low temperature (a) and high temperature (b) regions. Very similar values occur for the three lowest levels, with these differing simply in their directions. Moreover, these g-values are almost identical for the two potential surfaces, confirming that the temperature dependence of the orthorhombic component of the lattice strain has little effect on the composition of the wave functions. The main effect of the different value of the orthorhombic strain used to fit the higher temperature g-values is to slightly shift the relative energies of the vibronic levels. For the potential surface at low temperature, the g-values of levels 4 and 5 are quite similar to those of level 1, and those of level 6 are similar to those of level 2. This is consistent with these three higher levels approximating closely to upper vibrational states of the lowest pair of

(32) Bir, G.I. *Sov. Phys. Solid State* **1976**, *18*, 1627.

electronic states. However, the *g*-values of the potential surface at higher temperature do differ from those of the low temperature surface in one respect, namely that for levels 5 and 6 the two larger *g*-values are quite similar. This implies that the wave functions of these levels are significantly delocalized between the two lower minima of the potential surface. The delocalization occurs because the two levels, which correspond to upper vibrational states of the two lowest vibronic wave functions, are very close in energy. A similar effect has been reported for other "dynamic" copper(II) complexes.[5,9] Although such a delocalization has an insignificant effect on the temperature dependence of the *g*-values, it may possibly affect the rate of exchange between the lowest pair of energy levels. It may, therefore, influence the temperature dependence of the line shape of the EPR spectra, and we are currently investigating this aspect.

Interpretation Involving a Thermal Equilibrium between Orientation Isomers. Previous interpretations of the dynamic behavior of copper(II) complexes have often involved an equilibrium between two "orientation isomers" which have similar *g*-values and bond lengths, but with the directions of the largest and intermediate *g*-values, and associated bond lengths, interchanged in the crystal lattice; Silver and Getz developed a model based on this assumption.[3] This approach has been used to interpret the temperature dependence of the two higher *g*-values[6,7] and metal−ligand bond lengths[33] of a range of complexes. The magnitudes of the *g*-values of the first three vibronic levels are quite similar (Table 5), suggesting that the Silver−Getz approach should be valid, so it is of interest to extend the treatment to the present system where all three *g*-values change with temperature. Following Silver and Getz and Petrashen et al.,[3,6] the molecular *g*-values of the complex are given by

$$g_x(T) = K_1 g_{x1} + K_2 g_{y2} + K_3 g_{y3}$$

$$g_y(T) = K_1 g_{y1} + K_2 g_{x2} + K_3 g_{z3}$$

$$g_z(T) = K_1 g_{z1} + K_2 g_{z2} + K_3 g_{x3} \qquad (5)$$

Here, K_i is the fractional population in level i determined by Boltzmann statistics, $g_x(T)$ is the *g*-value of the complex as a whole at temperature T, and g_{xi} and so forth are the *g*-values of the levels $i = 1, 2, 3$. The subscripts *z*, *y*, and *x* refer to the *g*-values along the shortest, middle, and longest Cu−O bonds, respectively. As discussed previously,[5] this choice of the molecular coordinate system results from the fact that the principal symmetry axis of the system is provided by the axial strain. Equation 5 suggests that the temperature dependence of the *g*-values depends on just two parameters, the energies E_{12} and E_{13} of the two upper levels relative to the lowest level. Taking values for g_x, g_y, and g_z equal to those observed at low temperature for $Cs_2\{Zn[Cu](H_2O)_6\}(ZrF_6)_2$, the least-squares fit shown in Figure 8a yields the energies $E_{12} = 85$ cm^{-1} and $E_{13} = 180$ cm^{-1}. For this, although the behavior of the smallest *g*-value is reproduced satisfactorily, that of the two larger *g*-values is not, as these converge more rapidly than is predicted by eq 5. However, the observed behavior can be reproduced reasonably well, if it is assumed that the energy of the first excited level decreases linearly with temperature; that is, $E_{12} = (E_{12}^* - \delta T)$. The least-squares fit to eq 5 with this relationship substituted into the Boltzmann expressions (Figure 8b) yields the "best-fit" estimates $E_{12}^* = 90$ cm^{-1}, $\delta = 0.2$ cm^{-1} K^{-1}, and $E_{13} = 180$ cm^{-1}. A minor discrepancy remains as the two larger *g*-values are slightly overestimated at high temperature. This is presumably due to the neglect of other higher vibronic states in the treatment, because this aspect is reproduced satisfactorily in the more complete model (solid curve, Figure 4). However, it is apparent that the *g*-values of $Cs_2\{Zn[Cu](H_2O)_6\}(ZrF_6)_2$ may be reproduced quite well assuming a thermal equilibrium between three "orientation isomers" with the proviso that the energy difference between those involving a switch in direction of the two larger *g*-values decreases linearly as the temperature is raised. The treatment implies an energy separation of the two lowest levels of 84 cm^{-1} at 30 K and 30 cm^{-1} at 300 K. This agrees well with the separations 82 and 32 cm^{-1} estimated for the potential surface at low and high temperature using the more complete model of vibronic coupling (Table 5). The same is true for the energy separation of the first and third levels, which is 180 cm^{-1} using the Silver−Getz type approach and 190 and 165 cm^{-1} for the low and high-temperature potential surfaces of the more complete model.

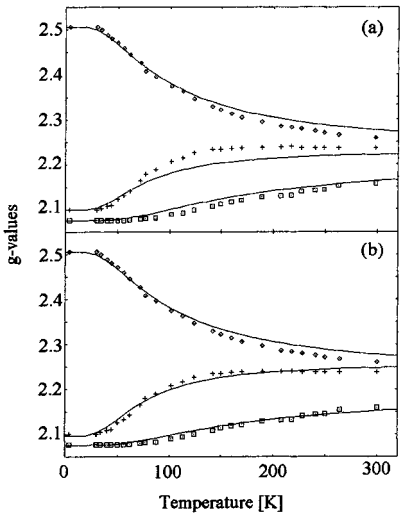

Figure 8. (a) Least-squares fit to the *g*-values of $Cs_2\{Zn[Cu](H_2O)_6\}(ZrF_6)_2$ assuming a Boltzmann distribution to three energy levels differing only in the orientation of the **g**-tensors. Part (b) is like part (a) but with the energy of the first excited level varying linearly with temperature. See text for the method of calculation.

Conclusions

The variation of the EPR spectrum of ~1% Cu^{2+} doped into $Cs_2[Zn(H_2O)_6](ZrF_6)_2$ can be interpreted satisfactorily using a potential surface perturbed by Jahn−Teller vibronic coupling and the influence of lattice strain interactions. The temperature dependence of the *g*-values and the variation of the EPR line shape with temperature both suggest that the lattice strain interactions are rather weak, considerably

(33) Simmons, C. *New. J. Chem.* **1993**, *17*, 77 and references therein.

smaller than those derived previously for Cu^{2+} doped into several Tutton salts of general formula $(cation)_2[Zn(H_2O)_6](SO_4)_2$. Moreover, it appears that the orthorhombic component of the strain decreases somewhat between 4.2 and 300 K. The crystal structure of $Cs_2[Zn(H_2O)_6](ZrF_6)_2$ confirms that the lattice perturbations acting on the $Zn(H_2O)_6^{2+}$ ion are quite small, as this has an almost regular octahedral geometry. The orientation of the **g**-tensor shows that the lattice strain interactions acting on the guest $Cu(H_2O)_6^{2+}$ ion are somewhat different from those perturbing the host zinc(II) complex.

To a good approximation, each of the three lowest vibronic wave functions deduced for the $Cu(H_2O)_6^{2+}$ ion in $Cs_2[Zn(H_2O)_6](ZrF_6)_2$ correspond to the same tetragonally elongated octahedral geometry with a slight orthorhombic distortion, but with the long axis of the Jahn−Teller distortion and largest *g*-value directed to a different pair of oxygen atoms. The *g*-values vary with temperature because of a thermal equilibrium between these energy levels. The rate of exchange between the energy levels is always fast enough that an average *g*-value is observed; though, at Q-band frequency, the EPR signals associated with the two higher *g*-values almost disappear at ∼80 K, suggesting that here the rate of exchange is almost equal to the microwave frequency. In future experiments, it is proposed to study this aspect by measuring the temperature dependence of the EPR spectra of single crystals at several microwave frequencies.

Acknowledgment. We thank Dr. R. L. Davidovich from the Institute of Chemistry, Vladivostok, for providing the crystals used in the initial parts of this study. Financial assistance from the Australian Research Commission is acknowledged by M.A.H. and H.S. This work was partly supported by the Scientific Committee under Grant KBN-2 PO3B 133 18.

IC010464D